Efficient OPF Calculations for Power System Reliability Assessment Based on State Similarity

Zeyu Liu[a,b], Jiawei Qu[a,b], Kai Hou[a,b]*,Yue Zhou[a,c], Hongjie Jia[a,b], Ruifeng Zhao[d], Shiqian Ma[c],' Xinzhe Wei[f]

[a]*Key Laboratory of Smart Grid of Ministry of Education, Tianjin University, Tianjin 300072, China*

[b]*Key Laboratory of Smart Energy & Information Technology of Tianjin Municipality, Tianjin 300072, China*

[c]*School of Engineering, Cardiff University, Cardiff CF24 3AA, U.K.*

[d] *Guangdong Power Grid Corp Power Dispatching Control Center, Guangzhou 510000, China*

[e]*State Grid Tianjin Electric Power Research Institute, Tianjin 300072, China*

[f]*State Grid Tianjin Electric Power Company Chengdong Branch, Tianjin 300072, China*

E-mail: * khou@tju.edu.cn

First Author information:

Zeyu Liu was born in Hebei province, China. He is currently doing postdoctoral research at Tianjin University. His research interest is reliability assessment.

Detailed address: Room A/303, Chengjiao Building, Tianjin University, Weijin Road No.92, Tianjin, 300072, China,

Email: tjulzy@tju.edu.cn, Tel: +86-18222952589

This work was financially funded by the National Natural Science Foundation of China program (Grant No. U23B6006/ U2066211) and China Postdoctoral Science Foundation Funded Project (Grant No. 2024M762353).

Highlights:

1) A state-similarity method transforms repeated DC OPF into linear equation solving.
2) A criterion is established to ensure the optimality of the equation solving.
3) A unified acceleration framework matches all system states.
4) A dynamic sorting strategy is proposed to further accelerate the assessment process.

Efficient OPF Calculations for Power System Reliability Assessment Based on State Similarity

Zeyu Liu[a,b], Jiawei Qu[a,b], Kai Hou[a,b]*,Yue Zhou[a,c], Hongjie Jia[a,b], Ruifeng Zhao[d], Shiqian Ma[e],' Xinzhe Wei[f]

[a]*Key Laboratory of Smart Grid of Ministry of Education, Tianjin University, Tianjin 300072, China*
[b]*Key Laboratory of Smart Energy & Information Technology of Tianjin Municipality, Tianjin 300072, China*
[c]*School of Engineering, Cardiff University, Cardiff CF24 3AA, U.K.*
[d] *Guangdong Power Grid Corp Power Dispatching Control Center, Guangzhou 510000, China*
[e]*State Grid Tianjin Electric Power Research Institute, Tianjin 300072, China*
[f] *State Grid Tianjin Electric Power Company Chengdong Branch, Tianjin 300072, China*

Abstract: As power systems grow more complex and integrate intermittent renewable energy sources, assessing system reliability has become increasingly time-consuming. A significant challenge arises from the repetitive calculations of optimal power flow (OPF), which minimizes load curtailment. To address this, a state-similarity-based method is proposed to accelerate the OPF calculations for reliability assessment. It is based on the observation that many states in reliability assessment exhibit similar OPF solutions with identical active constraints. This similarity allows system states to be grouped into categories, with each category containing states sharing the same active constraints. For states within the same category, the optimal load curtailment can be calculated by solving linear equations instead of optimization algorithms. Furthermore, optimality conditions are employed to ensure that states are accurately matched to their respective similarity categories. Also, this method can be conveniently integrated with the impact increment and cross-entropy methods for further efficiency improvements. Case studies conducted on the RTS-79, RTS-96, and Brazilian systems demonstrate that the proposed method significantly improves computational efficiency without sacrificing accuracy, when compared with traditional methods.

Keywords: Reliability Assessment, Power System, Renewable Energy, State Similarity, Active Constraints, Optimal Load Curtailment.

Nomenclature

Abbreviation

OPF	optimal power flow	AC	alternating current
REG	renewable energy generation	DC	direct current
WT	wind turbines	EENS	expected energy not supplied
PV	photovoltaics	LP	linear programming
SE	state enumeration	CR	category rank
MCS	Monte Carlo simulation	CEMCS	CE-based MCS method
IISE	impact-increment-based SE	SSMCS	SS-based MCS method
CE	cross-entropy	SSCEMCS	SS-based CEMCS method
SA	sensitivity analysis	SSSE	SS-based SE method
POA	post optimal analysis	SSIISE	SS-based IISE method
MPLP	multi-parametric linear programming	LR	load and renewable generation
LM	Lagrange multipliers	TL	transmission line
SS	state similarity approach	G	generation

Indices and Sets

Ω_s	the set of system state	k	the index of state
Ω_{CS}	the set of component state	l	the index of branch
Ω_{LG}	the set of load and generation state	i_{ss}	the index of similarity category
Ω_{ss}	the set of state similarity	i / j	the index of buses

Parameters and Constants

$\boldsymbol{s}$	system state	$\boldsymbol{Y}_t$	branch admittance matrices for the to ends
$\boldsymbol{s}_l$	branch state		
$\boldsymbol{s}_g$	generation state	$\boldsymbol{F}_{\max}$	the limit of branch power flow
$\boldsymbol{P}_d$	load level vector for buses	n_l	the number of branches
$\boldsymbol{P}_{\text{gmax}}$	maximum output vector for generators	n_g	the number of traditional generators
		n_b	the number of buses
n_{RE}	The number of renewable energy generators	$N_{ss\max}$	maximum allowable number of similarity categories
n_w	the number of WTs	N_{tri}	threshold for triggering the sorting operation
n_p	the number of PVs		
n_t	the number of load and generation states	$\Delta\boldsymbol{P}_{\text{gmax}}$	fluctuations in renewable generation outputs
$\boldsymbol{Y}_{bus}$	bus admittance matrix	$\Delta\boldsymbol{P}_d$	fluctuations in load levels
$\boldsymbol{C}_g$	generator connection matrix	$\boldsymbol{c}_{LC}$	cost of load curtailment
$\boldsymbol{Y}_f$	branch admittance matrices for the from ends		

Variables

f_{LC}	objective function	$\boldsymbol{y}_g$	slack variables of generation output
$\boldsymbol{\theta}$	bus angle	$\boldsymbol{y}_f$	slack variables of branch power flow for the from ends
$\boldsymbol{P}_g$	generation output		
$\boldsymbol{P}_{LC}$	load curtailment	$\boldsymbol{y}_t$	slack variables of branch power flow for the to ends
$\boldsymbol{\theta}'/\boldsymbol{\theta}''$	non-negative variables of bus angle		
$\boldsymbol{y}_{LC}$	slack variables of load curtailment		

1. Introduction

Renewable energy generation (REG), such as wind turbines (WT) and photovoltaics (PV), has been increasingly integrated into power systems [1]-[4]. However, the intermittency of REG can pose significant challenges to the stability and reliability of power systems[5]-[7]. Therefore, it is essential to evaluate the reliability of power systems

with REG for guiding their expansion in planning and operation.

Reliability assessment is a critical factor in determining the quality of power supply to users, and it typically involves three key processes [8]: system state selection, system state analysis, and reliability indices computation. The reliability indices are calculated based on the probability and impact (e.g., load curtailment) of system states over a specified period [9]. The number of system states will increase exponentially when considering REG fluctuations, component outages, and load variations, which can impose a significant computational burden on reliability assessment. As a result, improving computational efficiency of reliability assessment methods is crucial.

There are two elementary reliability assessment methods [10]: State Enumeration (SE) and Monte Carlo Simulation (MCS). SE can provide accurate reliability indices by explicitly or implicitly enumerating all possible system states. This method is attractive because it can mathematically reflect the relationship between reliability and system states. However, the SE method becomes inefficient in large-scale systems due to the exponential growth of system states [11]. To improve the computational efficiency of SE, various techniques have been proposed in recent years to reduce system states, such as the fast sorting algorithm [12], fast contingency screening technique [13], and impact-increment-based SE (IISE) method [14].

The MCS method selects system states according to their probability distribution and then estimates the reliability indices. Compared with SE, MCS is widely used in large-size systems [15]-[17]. Nevertheless, a large number of samples still lead to an extremely large computational effort, especially in power systems with low failure probabilities [18]. To this end, several variance reduction techniques have been employed to re-duce the samples of MCS, including importance sampling [19], Latin hypercube sampling [20], continuous-time Markov chain model [21], subset simulation [22], and cross-entropy (CE) method [23], etc.

The aforementioned methods primarily aim to reduce the number of system states to be analyzed. However, computational efforts in state analysis depend not only on the number of system states but also on the complexity of their analysis. Consequently, many scholars have investigated accelerating system state analysis by employing alternatives to OPF, such as deep learning methods [24], [25]. For example, Van et al. [26] proposed a reliability assessment method based on a graph convolutional neural network, in which a graph isomorphism network is introduced to capture the features of system edges and nodes. This method achieves a computational speed up to 1000 times faster than conventional model-driven approaches. Furthermore, to address the issue of topological

changes in reliability assessment, a multi-core collaborative GCN was proposed and integrated with a self-attention mechanism, enhancing its robustness in adapting to changing topologies [27]. However, the enhanced performance of these methods has only been validated on specific test sets and lacks proven accuracy, posing a significant challenge in safety-critical fields such as reliability assessments [28].

For numerous OPF computations in reliability assessment, further advancement in optimization-based methods remain crucial. Many studies in reliability assessment have demonstrated that optimal load curtailment across system states exhibits significant similarity, primarily due to limited variations in component outages, load levels, and REG outputs [29]. This similarity is leveraged to enhance the efficiency of OPF calculations. In many cases, it allows for directly obtaining the optimal solution, thereby replacing traditional optimization methods, as shown in Table I. The Sensitivity Analysis (SA) method is used to quantify the change in optimal load curtailment resulting from load variations [30]. Fotuhi-Firuzabad et al. [31] used the Post Optimal Analysis (POA) to exploit the similarity among different states and accelerate the evaluations of similar states. Kang et al. [32] proposed a multi-parametric linear programming (MPLP) method to reduce OPF computations. Generator outages and load variations are treated as MPLP parameters. This enables efficient analysis of massive system states by grouping them according to their identical optimal basis matrices. Qu et al. [33] extended this algorithm to the mixed-integer programming. By establishing a hierarchical solving mechanism and grouping integer variables, they achieved effective grouping of massive operation states.

However, transmission line outages remain a significant challenge. To address this, Liu et al. [34] introduced Lagrange multipliers to establish the relationship between optimal load curtailment and topological changes. By matching topological states with Lagrange multipliers based on similarity, they significantly improved the computational speed of reliability assessments. Luo et al. [35] proposed a reliability assessment method based on an improved failure effect occurrence matrix, enabling rapid optimal load shedding analysis by constructing failure components of topological and load states. For the numerous nonlinear OPF computations in reliability assessments, a nonlinear solution method based on KKT conditions and active constraints has been proposed [36]. This approach transforms the nonlinear OPF problem into an underdetermined system of equations, solving it iteratively to improve computational efficiency. Since the KKT conditions are necessary but not sufficient, this method cannot guarantee a globally optimal solution. Our previous work [37] used Lagrange Multipliers (LM) to derive the linear

relationship between the optimal load curtailment and the variations of load and REG. However, these methods are not applicable in cases of transmission line outages, where the system topology and state similarities may change. Since all line outage states must be analyzed by optimization methods, this remains a considerable computational burden, especially for large-scale systems [34]. Moreover, the matching processes of state similarity require significant computational resources, and the efficiency of these processes needs further enhancement.

Table. I Previous studies on state similarity

Methods	State Similarity Features	Accelerated State				Speedup*
		Component Outages		Variations		
		TL	G	Load	REG	
SA [30]	Optimal basis	-	-	√	-	≈2.33
POA [31]	Original solution	-	√	√	-	1~7
MPLP [32]	Optimal basis	-	√	√	-	23~30
LM [37]	Lagrange multipliers	-	-	√	√	>20

* Speedup represents the multiple for efficiency improvement.

This paper proposes a state-similarity (SS) approach to accelerate system state analysis in reliability assessment. In this approach, the active constraints of optimal power flow (OPF) problems are employed as distinctive features to characterize the similarities among different system states. Two system states are regarded as state-similar if they share identical sets of active constraints. Based on this property, the proposed method enables the optimal load curtailment to be directly derived by solving a set of linear equations, without invoking iterative optimization algorithms. Consequently, the proposed method can significantly improve the computational efficiency for reliability assessment. The main contributions are as follows:

- This paper proposes a state-similarity-based method to enhance the efficiency of reliability assessments in power systems. By identifying similarities among numerous system states, the OPF optimization problem is transformed into a task of solving linear equations. For OPF problems within the same state similarity category, only one optimization is required, while the optimal load curtailment for other states can be efficiently derived by solving linear equations.
- A unified acceleration framework is developed to cover all types of system states. By leveraging active constraints as similarity features, this framework in-corporates line outage states with diverse topologies into the matching scope of state similarity.
- Optimality conditions ensure accurate matching of each state to its corresponding similarity category. Additionally, a dynamic sorting technique enhances the efficiency of the matching process.

The rest is organized as follows: Section 2 gives the problem statement and solution framework. Section 3

136 introduces the proposed SS method. Case studies are performed in Section 4 and conclusions are drawn in Section
137 5.

138 2. Problem Statement and Solution Framework

139 *2.1. Reliability Assessment of Power Systems*

140 Reliability assessment evaluates not only the likelihood of failure events but also the severity of their
141 consequences. It generally involves three steps, as shown in Fig. 1.

142 **Step 1**: *System state selection*.

143 The first step is the selection of system states and the calculation of their probabilities. Two fundamental
144 methods are commonly used for state selection: state enumeration (SE) and Monte Carlo simulation (MCS).

145 The system states are associated with component states, load levels, and REG outputs, which can be expressed
146 as follows,

147
$$\boldsymbol{s} = \left[\boldsymbol{s}_l \ \boldsymbol{s}_g \ \boldsymbol{P}_d \ \boldsymbol{P}_{g\max} \right] \tag{1}$$

148 where $\boldsymbol{s}$ is a system state; $\boldsymbol{s}_l$ denotes the branch state, composed of state variables for n_l branches; $\boldsymbol{s}_g$ denotes the
149 generation state, composed of state variables for n_g generators. The n_g generators comprise both traditional
150 generators and n_{RE} renewable energy generators, where n_{RE} units consists of n_w WTs and n_p PVs. In Fig. 1, $\boldsymbol{s}_k$
151 represents the k-th system state in the system state set Ω_s, $[\boldsymbol{s}_l \ \boldsymbol{s}_g]_k$ represents the k-th component state in the
152 component state set Ω_{CS}, and $[\boldsymbol{P}_d \ \boldsymbol{P}_{g\max}]_k$ represents the k-th load and generation state in the load and generation
153 state set Ω_{LG}. The number of load and generation states is denoted as n_t, which generally corresponds to 8760 for a
154 one-year time frame.

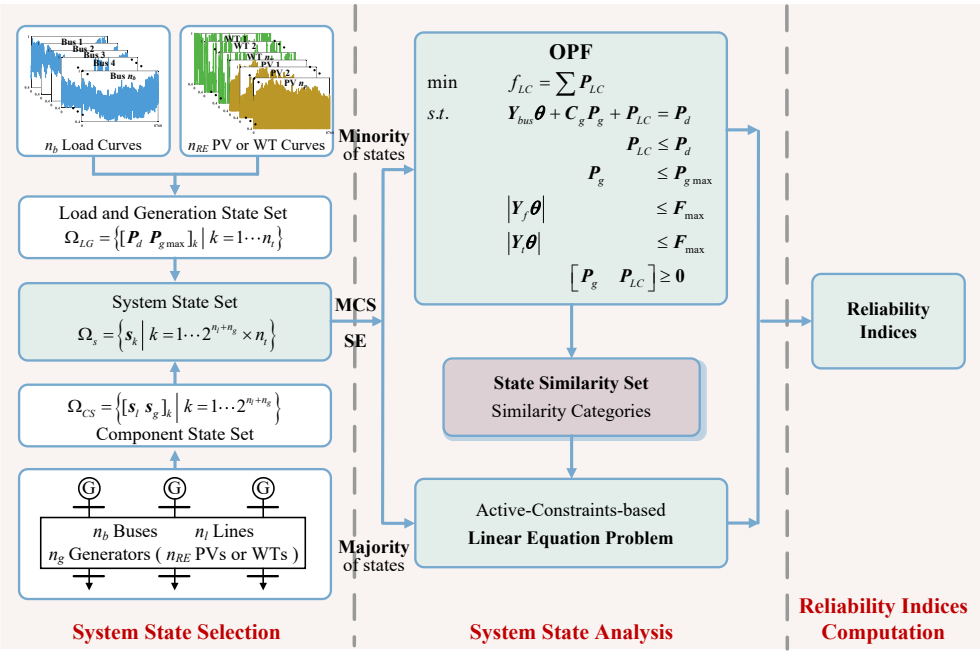

Fig. 1 Framework of the proposed state-similarity-based reliability assessment method.

Step 2: *System state analysis*.

In the second step, OPF is performed to analyze each system state and assess its consequence. OPF is used to reschedule generators and alleviate the violation of constraints, while minimizing the total load curtailment if unavoidable. Both alternating current (AC) and direct current (DC) power flow models can be embedded in OPF. The AC model can provide highly accurate results that closely align with real-world scenarios, but requires significant computational resources and may encounter severe convergence issues [38]. On the other hand, the DC model linearizes power flow equations, making it suitable for large-scale simulations and analysis of various failure states [39]. Although its accuracy is lower, it is generally acceptable for planning purposes. As a result, the DC OPF model is commonly adopted in the reliability assessment of power systems [18], [32], [40], [41]. It can be formulated as follows,

$$
\begin{aligned}
\min\quad & f_{LC}=\sum \boldsymbol{P}_{LC} \\
s.t.\quad & \boldsymbol{Y}_{bus}\boldsymbol{\theta}+\boldsymbol{C}_g\boldsymbol{P}_g+\boldsymbol{P}_{LC}=\boldsymbol{P}_d \\
& \boldsymbol{P}_{LC}\le\boldsymbol{P}_d \\
& \boldsymbol{P}_g\le\boldsymbol{P}_{g\max} \\
& |\boldsymbol{Y}_f\boldsymbol{\theta}|\le\boldsymbol{F}_{\max} \\
& |\boldsymbol{Y}_t\boldsymbol{\theta}|\le\boldsymbol{F}_{\max} \\
& \boldsymbol{P}_g,\boldsymbol{P}_{LC}\in\mathbb{R}^+,\boldsymbol{\theta}\in\mathbb{R}
\end{aligned}
\tag{2}
$$

Step 3: *Reliability indices computation*.

The reliability indices are usually determined based on the load curtailments of system states and their occurrent probabilities. In this study, expected energy not supplied (EENS) is adopted as the reliability index.

2.2. Challenges and Proposed Solution Framework

During the state selection process, some improved SE or MCS techniques have been applied to reduce the number of system states. However, the OPF problem (2) should be calculated for each system state, posing great computational challenges for large-scale power systems with large numbers of system states. Therefore, analyzing enormous numbers of states is still a time-consuming impediment to reliability assessment.

Generally, the OPF problem (2) associated with many states may share the same active constraints. This shared characteristic can be exploited as a state similarity to solve a set of similar OPF problems with minimal effort. Instead of applying optimization algorithms to solve each similar problem, active constraints can be used to transform the original OPF problem into a linear equations problem, significantly accelerating the state analysis process.

Consequently, the active-constraints-based linear equations is constructed as an alternative approach to solving OPF problems. As shown in Fig. 1, a few states are solved using traditional optimization algorithms, and their respective active constraints are stored in the state similarity set. Each of these states represent a specific state similarity category. For the remaining states, their state similarity categories are identified based on their active constraints, allowing their solutions to be efficiently computed by solving linear equations, thereby enhancing the efficiency of reliability assessment.

3. Proposed State-Similarity Approach

3.1. State Similarity in the LP Problem

The DC OPF problem (2) is a typical linear programming (LP) problem. An LP problem can be expressed in a standard form,

$$\begin{aligned} \min \quad & f = \boldsymbol{c}\boldsymbol{x} \\ s.t. \quad & \boldsymbol{A}\boldsymbol{x} = \boldsymbol{b} \\ & \boldsymbol{x} \geq \boldsymbol{0} \end{aligned} \tag{3}$$

where $\boldsymbol{A} \in \mathbb{R}^{m \times n}$, $\boldsymbol{b} \in \mathbb{R}^{m}$ and $\boldsymbol{c} \in \mathbb{R}^{n}$ are given, and $\boldsymbol{x} \in \mathbb{R}^{n}$ is a vector of variables to minimize the objective $f : \mathbb{R}^{n} \to \mathbb{R}$. A feasible solution is a non-negative vector of the variables $\boldsymbol{x}$ that satisfies the constraints of (3). Among feasible solutions, the one that minimizes the *f* is the *optimal solution*.

Theorem 1 [42]: An optimal solution of LP problem lies at the intersection point of *n* constraints. In this study, these constraints are referred to as the *active constraints*, which can be represented as follows,

$$\begin{cases} \boldsymbol{A}\boldsymbol{x} = \boldsymbol{b} & m \quad constraints \\ \boldsymbol{x}_a = \boldsymbol{0} & (n-m) \ constraints \end{cases} \tag{4}$$

where $\boldsymbol{x}_a$ represent the *active variables*, which are specifically composed of *n-m* variables.

For example, Fig. 2(a) presents an LP problem that has 6 active constraints at the optimal solution. The active constraints are as follows,

$$\begin{cases} \begin{bmatrix} 1 & 1 & 1 & 0 & 0 & 0 \\ 1 & -1 & 0 & -1 & 0 & 0 \\ 1 & 1 & 0 & 0 & -1 & 0 \\ 1 & -1 & 0 & 0 & 0 & 1 \end{bmatrix} \boldsymbol{x} = \begin{bmatrix} 4 \\ -1 \\ 2 \\ 1 \end{bmatrix} \\ \boldsymbol{x}_a = \begin{bmatrix} x_3 & x_4 \end{bmatrix}^T = \boldsymbol{0} \end{cases} \tag{5}$$

Based on the simplex method [42], the *active variables* $\boldsymbol{x}_a$ correspond to the *non-basic variables* $\boldsymbol{x}_N$, while the remaining variables classified as the *basic variables* $\boldsymbol{x}_B$. This allows us to partition $\boldsymbol{A}$ and $\boldsymbol{c}$ into ($\boldsymbol{B}$, $\boldsymbol{N}$) and ($\boldsymbol{c}_B$, $\boldsymbol{c}_N$), respectively. As a result, the LP problem (3) can be simplified into the system of linear equations (6), denoted as *F*(*x*),

$$F(\boldsymbol{x}) = \begin{bmatrix} \boldsymbol{A}\boldsymbol{x} = \boldsymbol{b} \\ \boldsymbol{x}_a = \boldsymbol{0} \end{bmatrix} = \begin{bmatrix} \boldsymbol{B}\boldsymbol{x}_B = \boldsymbol{b} \\ \boldsymbol{x}_a = \boldsymbol{0} \end{bmatrix} \tag{6}$$

where $\boldsymbol{B}$ is a basis matrix. The solution of LP is,

$$\boldsymbol{x} = \begin{bmatrix} \boldsymbol{x}_B & \boldsymbol{x}_a \end{bmatrix}^T = \begin{bmatrix} \boldsymbol{B}^{-1}\boldsymbol{b} & \boldsymbol{0}_{1 \times (n-m)} \end{bmatrix}^T \tag{7}$$

Theorem 2 [42] (optimality conditions): The solution (7) is an optimal solution to the LP problem (3) if:

$$\boldsymbol{B}^{-1}\boldsymbol{b} \geq \boldsymbol{0} \tag{8}$$

$$\boldsymbol{c}_N - \boldsymbol{c}_B\boldsymbol{B}^{-1}\boldsymbol{N} \geq \boldsymbol{0} \tag{9}$$

Equations (8) and (9) are the optimality conditions that the basis matrix $\boldsymbol{B}$ must satisfy to ensure an optimal solution. In addition, according to the definition of state similarity, these equations can also be employed as criteria for determining whether two optimization problems are state-similar. Specifically, if the basis matrix $\boldsymbol{B}$ obtained

from the original problem also satisfies the optimality conditions defined by Eqs. (8) and (9) in the new problem, the two problems are regarded as state-similar. In such cases, the optimal solution of the new problem can be directly derived from Eq. (7) without re-solving the optimization problem. Otherwise, the problems are not considered state-similar.

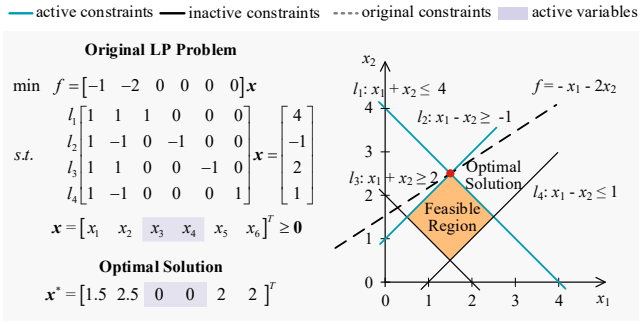

(a) the original LP problem

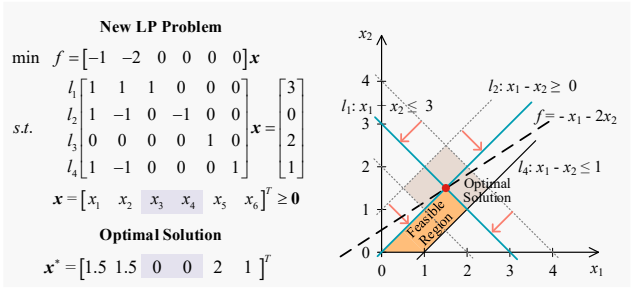

(b) the new LP problem

Fig. 2. An example of state similarity between LP problems. (a) represents the original optimization problem, and (b) represents a new optimization problem formed by altering the right-hand side vector $\boldsymbol{b}$ and the coefficient matrix $\boldsymbol{A}$ of the original problem. These two problems have entirely different feasible regions. The relationship between them is that they share the same active constraints, despite the change in $\boldsymbol{A}$ and $\boldsymbol{b}$. As defined in Eq.(4), l_1, l_2, l_3, l_4, x_3=0, and x_4=0 are active constraints. Furthermore, x_3 and x_4 are also the active variables. When the problem is represented in the two-dimensional plane of x_1 and x_2, only two active constraints emerge, and the optimal solution is located precisely at their intersection. In the new LP problem (b), the active constraints l_1, l_2, l_3, l_4, along with x_3=0, and x_4=0, are maintained. Therefore, even when $\boldsymbol{A}$ and $\boldsymbol{b}$ change, the new LP problem shares the same active constraints as the original problem, and can be efficiently solved by the active-constraints-based linear equations.

As shown in Fig. 2, despite differences in the constraints between the original and new LP problem, they share identical active variables (i.e., $x_3 = 0$ and $x_4 = 0$). Therefore, the new LP problem can be transformed into a system of linear equations based on these active constraints. Using the active constraints provided by original states, the optimal solution to the new LP problem can be directly obtained through (10), eliminating the need for optimization algorithms.

$$\boldsymbol{x}_B^* = \begin{bmatrix} x_1 \\ x_2 \\ x_5 \\ x_6 \end{bmatrix} = \begin{bmatrix} 1 & 1 & 0 & 0 \\ 1 & -1 & 0 & 0 \\ 0 & 0 & 1 & 0 \\ 1 & -1 & 0 & 1 \end{bmatrix}^{-1} \begin{bmatrix} 3 \\ 0 \\ 2 \\ 1 \end{bmatrix} = \begin{bmatrix} 1.5 \\ 1.5 \\ 2 \\ 1 \end{bmatrix}$$
$$\boldsymbol{x}_N^* = \begin{bmatrix} x_3 \\ x_4 \end{bmatrix} = \begin{bmatrix} 0 \\ 0 \end{bmatrix} \tag{10}$$

Consequently, *state similarity* is defined as a condition in which LP problems share the same active constraints at their respective solutions, regardless of variations in the parameters of LP problems. In many practical scenarios, many new LP problems are only slightly different from the original LP problem, and are likely to share the same active constraints. While optimization algorithms are the most straightforward method for solving new LP problems, solving them using the active-constraints-based linear equations (6) is more efficient, as long as the optimality conditions (8) and (9) are satisfied.

3.2. State Similarity in the DC OPF Problem

In the reliability assessment, the evaluation process requires repeatedly solving DC OPF problems for different states. The DC OPF problem (2) can be expressed in the standard form (3),

$$\begin{aligned} \min \quad & f_{LC} = \boldsymbol{c}_{LC} \sum \boldsymbol{P}_{LC} \\ s.t. \quad & \boldsymbol{Y}_{bus}\boldsymbol{\theta} + \boldsymbol{C}_g \boldsymbol{P}_g + \boldsymbol{P}_{LC} = \boldsymbol{P}_d \\ & \boldsymbol{P}_{LC} + \boldsymbol{y}_{LC} = \boldsymbol{P}_d \\ & \boldsymbol{P}_g + \boldsymbol{y}_g = \boldsymbol{P}_{g\max} \\ & \left|\boldsymbol{Y}_f \boldsymbol{\theta}\right| + \boldsymbol{y}_f = \boldsymbol{F}_{\max} \\ & \left|\boldsymbol{Y}_t \boldsymbol{\theta}\right| + \boldsymbol{y}_t = \boldsymbol{F}_{\max} \\ & \begin{bmatrix} \boldsymbol{\theta}' & \boldsymbol{\theta}'' & \boldsymbol{P}_g & \boldsymbol{P}_{LC} & \boldsymbol{y}_{LC} & \boldsymbol{y}_g & \boldsymbol{y}_f & \boldsymbol{y}_t \end{bmatrix}^{\mathrm{T}} \in \mathbb{R}^+ \end{aligned} \tag{11}$$

Following the standard form of LP problem, the $\boldsymbol{c}$, $\boldsymbol{A}$, $\boldsymbol{x}$, and $\boldsymbol{b}$ are,

$$\boldsymbol{c} = \boldsymbol{c}_{LC} \begin{bmatrix} \boldsymbol{0}_{1\times n_b} & \boldsymbol{I}_{1\times n_b} & \boldsymbol{0}_{1\times n_g} & \boldsymbol{0}_{1\times(n_g+n_b+2n_l)} \end{bmatrix} \tag{12}$$

$$\boldsymbol{A}=\left[\begin{array}{c|cc|cc|cc} \boldsymbol{Y}_{bus} & \boldsymbol{I}_{n_b\times n_b} & \boldsymbol{C}_g & \multicolumn{2}{c|}{\boldsymbol{0}} & \multicolumn{2}{c}{\boldsymbol{0}} \\ \hline \boldsymbol{0} & \boldsymbol{I}_{n_b\times n_b} & & \boldsymbol{I}_{n_b\times n_b} & & \multicolumn{2}{c}{\boldsymbol{0}} \\ & & \boldsymbol{I}_{n_g\times n_g} & & \boldsymbol{I}_{n_g\times n_g} & & \\ \hline \boldsymbol{Y}_f & \multicolumn{2}{c|}{\multirow{2}{*}{$\boldsymbol{0}$}} & \multicolumn{2}{c|}{\multirow{2}{*}{$\boldsymbol{0}$}} & \boldsymbol{I}_{n_l\times n_l} & \\ \boldsymbol{Y}_t & \multicolumn{2}{c|}{} & \multicolumn{2}{c|}{} & & \boldsymbol{I}_{n_l\times n_l} \end{array}\right] \tag{13}$$

$$\boldsymbol{x}=\left[\begin{array}{cc|cc|cc|cc} \boldsymbol{\theta}' & \boldsymbol{\theta}'' & \boldsymbol{P}_{LC} & \boldsymbol{P}_g & \boldsymbol{y}_{1\times n_b} & \boldsymbol{y}_{1\times n_g} & \boldsymbol{y}_{1\times n_l} & \boldsymbol{y}_{1\times n_l} \end{array}\right]^{\mathrm{T}} \tag{14}$$

$$\boldsymbol{b}=\left[\begin{array}{ccccc} \boldsymbol{P}_d & \boldsymbol{P}_d & \boldsymbol{P}_{g\max} & \boldsymbol{F}_{\max} & \boldsymbol{F}_{\max} \end{array}\right]^{\mathrm{T}} \tag{15}$$

where $\boldsymbol{I}$ is the identity matrix.

The active variables in the DC OPF problem are,

$$\boldsymbol{x}_a=\left[\begin{array}{cccccc} \boldsymbol{\theta}'_a & \boldsymbol{\theta}''_a & \boldsymbol{P}_{LC,a} & \boldsymbol{P}_{g,a} & \boldsymbol{y}_a \end{array}\right]^{\mathrm{T}}=\boldsymbol{0} \tag{16}$$

where $\boldsymbol{\theta}'_a$, $\boldsymbol{\theta}''_a$, $\boldsymbol{P}_{LC,a}$, $\boldsymbol{P}_{g,a}$, and $\boldsymbol{y}_a$ are the active variables in $\boldsymbol{x}$, and these variables are equal to 0.

During the state analysis process, variations in component states, load levels, and renewable generation outputs lead to different constraints. The $\tilde{\boldsymbol{b}}$ for diverse states is represented as,

$$\tilde{\boldsymbol{b}}=\left[\begin{array}{ccccc} \boldsymbol{P}_d+\Delta\boldsymbol{P}_d & \boldsymbol{P}_d+\Delta\boldsymbol{P}_d & \boldsymbol{P}_{g\max}+\Delta\boldsymbol{P}_{g\max} & \boldsymbol{F}_{\max} & \boldsymbol{F}_{\max} \end{array}\right]^{\mathrm{T}} \tag{17}$$

The branch outages can alter the system topology. If the l-th branch between the buses i and j fails, the $\tilde{\boldsymbol{A}}$ in the new DC OPF problem is,

$$\tilde{\boldsymbol{A}}=\begin{array}{c} \\ i \\ j \\ \\ l \\ n_l+l \end{array}\begin{array}{c} \begin{array}{ccccc} \quad & i & \quad & j & \quad \end{array} \\ \left[\begin{array}{ccccc} \cdots & Y_{ii}+\frac{1}{x_{ij}} & \cdots & Y_{ij}-\frac{1}{x_{ij}} & \cdots \\ \cdots & Y_{ji}-\frac{1}{x_{ji}} & \cdots & Y_{jj}+\frac{1}{x_{ji}} & \cdots \\ \vdots & & \vdots & & \vdots \\ & Y_{li}-\frac{1}{x_{ij}} & & Y_{lj}+\frac{1}{x_{ij}} & \\ & Y_{li}+\frac{1}{x_{ij}} & & Y_{lj}-\frac{1}{x_{ij}} & \end{array}\right] \end{array} \tag{18}$$

Therefore, in reliability assessment, the discrepancies between different system states are reflected in changes to the coefficient matrix $\boldsymbol{A}$ due to topological variations, as well as in alterations to the right-hand side vector $\boldsymbol{b}$ caused by fluctuations in generation and load. As illustrated in Fig. 2, assuming that the active constraints remain

unchanged, the DC OPF problem for a new state can be transformed into the following linear equations,

$$F\left(\boldsymbol{x}, \boldsymbol{x}_a = 0\right) = \begin{bmatrix} \tilde{\boldsymbol{A}}\boldsymbol{x} = \tilde{\boldsymbol{b}} \\ \boldsymbol{x}_a = \boldsymbol{0} \end{bmatrix} \Rightarrow \boldsymbol{x} = \begin{bmatrix} \boldsymbol{x}_B \\ \boldsymbol{x}_a \end{bmatrix} = \begin{bmatrix} \tilde{\boldsymbol{B}}^{-1}\tilde{\boldsymbol{b}} \\ \boldsymbol{0} \end{bmatrix} \tag{19}$$

Clearly, solving this system of linear equations involves matrix inversion. Equation (18) demonstrates that only a slight perturbation occurs in the basis $\tilde{\boldsymbol{B}}$, while most of the elements remain unchanged. Therefore, the original basis $\boldsymbol{B}$ from similar states can be reused to improve the efficiency of matrix inversion.

Theorem 3 [43] (Sherman-Morrison-Woodbury Formula): Consider a perturbation $\boldsymbol{UV}$, where $\boldsymbol{U}$ and $\boldsymbol{V}$ are matrices of size $m \times p$ and $p \times m$, respectively. If both $\boldsymbol{B}$ and $\boldsymbol{I} + \boldsymbol{V}\boldsymbol{B}^{-1}\boldsymbol{U}$ are nonsingular, then $\boldsymbol{B} + \boldsymbol{UV}$ is nonsingular, and the inverse of $\tilde{\boldsymbol{B}}$ is,

$$\tilde{\boldsymbol{B}}^{-1} = (\boldsymbol{B} + \boldsymbol{UV})^{-1} = \boldsymbol{B}^{-1} - \boldsymbol{B}^{-1}\boldsymbol{U}(\boldsymbol{I} + \boldsymbol{V}\boldsymbol{B}^{-1}\boldsymbol{U})^{-1}\boldsymbol{V}\boldsymbol{B}^{-1} \tag{20}$$

According to (20), $\boldsymbol{U}$ and $\boldsymbol{V}$ are,

$$\boldsymbol{U} = \begin{array}{c} \\ i \\ j \\ \\ l \\ n_l + l \end{array} \begin{bmatrix} & & & & \\ 1 & & & & \\ & 1 & & & \\ & & & 1 & \\ & & & & 1 \\ & & & & \end{bmatrix}_{m \times p} \quad \boldsymbol{V} = \begin{array}{c} \begin{array}{cc} i & j \end{array} \\ \begin{bmatrix} \frac{1}{x_{ij}} & -\frac{1}{x_{ij}} \\ -\frac{1}{x_{ij}} & \frac{1}{x_{ij}} \\ -\frac{1}{x_{ij}} & \frac{1}{x_{ij}} \\ \frac{1}{x_{ij}} & -\frac{1}{x_{ij}} \end{bmatrix}_{p \times m} \end{array} \tag{21}$$

As shown in (21), this fast matrix inversion technique allows us to efficiently invert $\tilde{\boldsymbol{B}}$ in $O(m^2 + p^3)$ flops, as opposed to the conventional matrix inversion, which requires $O(m^3)$ flops.

In reliability assessment, when a new system state is encountered, its corresponding similarity category is initially unknown. To address this, the new state must be matched with an existing category in the state similarity set. This process follows a "hypothesize-and-verify" strategy: first, the new state is assumed to belong to a specific similarity category within the set. The relevant active constraints are then used to transform the DC OPF problem into a system of linear equations for efficient solution. Finally, optimality conditions (8) and (9) are applied to verify the solution. If the conditions are satisfied, the hypothesis is confirmed, and the new state is classified into the hypothesized similarity category, with the solution representing the optimal solution for the new state. If the optimality conditions are not met, the new state is then matched with other categories in the state similarity set, and this process continues until a successful match is found. If no category matches, it indicates that the new state does

not belong to any of the known similarity categories in the state similarity set, and optimization algorithms are employed to solve the OPF problem directly. The new state is then added to the state similarity set as a new category.

In summary, the proposed state-similarity-based approach is formulated in Algorithm 1.

Algorithm 1： State Similarity Approach for Solving DC OPF

Inputs: a new state s and the state similarity set Ω_{ss}
flag := 0, the similarity category order i_s := 1.
while flag = 0 **and** i_s <= count (similarity categories) **do**
  Choose the i_s-th similarity category from the state similarity set Ω_{ss} and obtain its active constraints.
  Calculate a solution $\boldsymbol{x}$ of s by linear equations (19).
  if the optimality conditions (8) and (9) are true **then**
    flag ← 1
    The optimal solution $\boldsymbol{x}^* = \boldsymbol{x}$.
  end
  $i_s = i_s + 1$.
end
if flag is false **then**
  The optimal solution $\boldsymbol{x}^*$ of the new state s is calculated by optimization algorithms.
  The new state s is stored as a new category in Ω_{ss}.
end
Outputs: The optimal solution $\boldsymbol{x}^*$ of the new state s

3.3. The State Similarity Set

The state similarity set, denoted as Ω_{ss}, consists of state similarity categories, each representing a group of states that share the same active constraints. Any given system state should match one of the categories in the set, meaning it belongs to the same similarity category and shares the same active constraints. There are four basic operations on Ω_{ss}:

1) *Matching*: Each state similarity category is sequentially traversed, and the active constraints of the representative state in the category are used to solve the DC OPF problem for the new state until the optimality conditions (8) and (9) are satisfied. If the new state does not match any existing categories, it will be analyzed using optimization algorithms, followed by an insertion operation described below.

2) *Insertion*: The new state, representing a new similarity category, is added to the beginning of Ω_{ss}. Its active constraints are then used to match subsequent new states in reliability assessment.

3) *Deletion*: When the number of state similarity categories in Ω_{ss} exceeds $N_{ss\max}$, the last state similarity category is removed. $N_{ss\max}$ is the maximum allowable number of similarity categories in the set.

4) *Sorting*: A dynamic sorting technique is developed to reorder the state similarity categories based on their Category Rank (CR), which will be explained later. The sorting operation is triggered only when a matched

category ranks higher than N_{tri}.

To enhance the matching efficiency, the state similarity categories that are more likely to match with the new states should be placed at the head of the set. In this study, CR is a numeric value that indicates the likelihood of a category matching a new state. In general, as more new states match with a category, the corresponding CR assigned to the category increases. The CR is calculated by,

$$CR(C)=\begin{cases} N_{u\max} & t-t_{ins}\le t_1 \\ N_u & t-t_{ins}>t_1, t-t_{last}<t_2 \\ 0 & t-t_{last}\ge t_2 \end{cases} \tag{22}$$

where C is a state similarity category in the set; t represents time, quantified by the number of analyzed states in the reliability assessment; N_u is the number of states that match this similarity category; $N_{u\max}$ is a large constant; t_{ins} is the time when the state similarity category is inserted into Ω_{ss}; t_{last} is the last matching time of the state similarity category; t_1 is the duration of the early-time region; t_2 is the maximum time after t_{last}. The CR of a state similarity category over time is shown in Fig. 3.

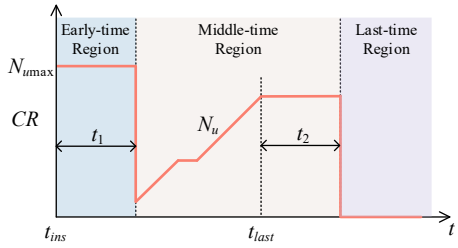

Fig. 3. An example of the state similairty between LP problems.

3.4. Proposed Reliability Assessment Method

The overall reliability assessment process using the proposed SS approach is outlined in Fig. 4 and explained as follows:

Step 1: Input system data, annual curves of loads and REGs, and preset parameters.

Step 2: Create the system state set Ω_s by MCS or SE.

Step 3: Select a system state s from Ω_s.

Step 4: Establish the DC OPF problem for the selected system state s as the standard form (11) - (15).

Step 5: Set the similarity category order i_{ss} = 1.

Step 6: Choose the i_{ss}-th similarity category from the state similarity set Ω_{ss}.

Step 7: Obtain the active variables x_a from the i_{ss}-th similarity category.

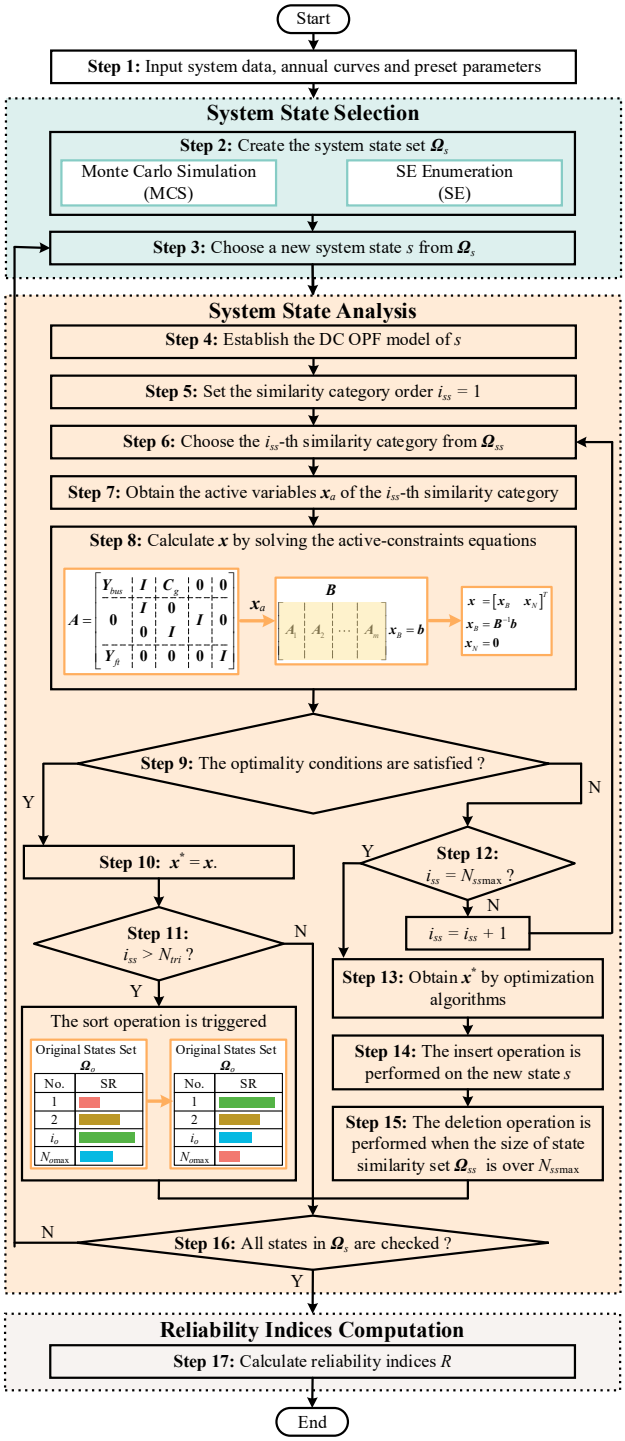

Fig. 4. The overall process of reliability assessment using the SS approach.

Step 8: Calculate a solution $\boldsymbol{x}$ of state $\boldsymbol{s}$ by solving the active-constraints-based linear equations instead of the DC OPF optimization.

Step 9: Check the optimality conditions of (8) and (9) to determine whether the solution $\boldsymbol{x}$ is the optimal solution.

If not, go to Step 12.

Step 10: The solution $\boldsymbol{x}$ is the optimal solution $\boldsymbol{x}^*$.

Step 11: Check if the trigger event $i_{ss} > N_{tri}$ occurs. If so, apply the dynamic sorting technique to reorder the state similarity set Ω_{ss}. Then, go to Step 16.

Step 12: Check if all state similarity categories in the state similarity set Ω_{ss} have been matched, i.e., $i_{ss} = N_{ss\max}$. If not, $i_{ss} = i_{ss} + 1$, go back to Step 6.

Step 13: Obtain the optimal solution $\boldsymbol{x}^*$ of state s by optimization algorithms.

Step 14: Treat state s as a new similarity category and insert it at the beginning of Ω_{ss}.

Step 15: Remove the last state similarity category from Ω_{ss} when the number of categories exceeds $N_{ss\max}$.

Step 16: Check if all states in Ω_s have been evaluated. If so, next Step, otherwise, go back to Step 3.

Step 17: Calculate reliability indices.

4. Numerical Results

The proposed SS approach is employed to evaluate the reliability of the RTS-79 [44], RTS-96 [45], and Brazilian systems [46]. The transmission limitations are considered. The cases utilize 17 actual annual load curves from Alberta [47], and 33 actual annual output curves for PV and WT from NREL [48], [49]. The maximum fluctuation range for both load data and renewable energy data is from 0 to 1.0. Moreover, different renewable generation penetrations are applied to analyze their impact on the system reliability. ζ_{re} is the renewable generation penetration, which is defined as,

$$\xi_{re} = \frac{P_{re}}{P_{cg} + P_{re}} \tag{23}$$

where P_{cg} and P_{re} represents the capacity of conventional generators and renewable generators, respectively; $P_{cg} + P_{re}$ is the total generation capacity.

MOSEK 9.3 is used as the optimization solver. The experiments are carried out on a standard PC equipped with Intel® Core® i5-10600KF CPU 4.10 GHz and 128 GB RAM using MATLAB® R2022a.

4.1. Case I: Results on the RTS-79 System

RTS-79 system [44] is a composite power system with 24 buses, 33 generator units, and 38 branches. The total

generation capacity is 3405 MW and the peak load is 2850 MW. The proposed method is verified by four cases with renewable generation penetrations of 0%, 5%, 10%, and 15%.

Two conventional methods, MCS and SE are utilized for comparisons. Moreover, the CE-based MCS (CEMCS) method and IISE method are also used for comparisons. The baseline of reliability assessment results is calculated by the MCS with 1×10^8 sampled states. The preset parameters are given as follows: N_T (maximum contingency order for SE) = 5, and β (the coefficient of variation for MCS) = 1%. In the SE method, the system states above second-order are only generation contingencies, which can cover 98.778 % of system states. In addition, the number of load and generation states in SE is reduced to 100 through the clustering technique.

The SSMCS, SSCEMCS, SSSE, and SSIISE methods are combinations of the proposed SS approach and MCS, CEMCS, SE, and IISE methods, respectively. The reliability assessment results of these methods are presented in Table II and Fig. 5.

In addition, the reliability level gradually declines owing to the intermittent nature of renewable energy. As shown in Table II, the efficiency of the SS method slightly decreases at higher renewable generation penetrations compared to lower penetrations. This is because the inherent variability of renewable energy causes changes in active constraints, making it more challenging to match a new state with the state similarity category. Although the OPF number increases with renewable generation penetration, SS method still significantly improves the efficiency.

4.1.1 Efficiency and Accuracy

First, the reliability indices obtained by SS methods exhibit the same precision while significantly improving computational efficiency. Compared with the SE and IISE methods, the proposed SS methods can increase the computational speed by 100~200 times. SE and IISE methods require over 20000 seconds to evaluate the RTS-79 system, while SSSE and SSIISE methods only take 100~200 seconds. Fig. 5 presents a comparative visualization of computational time and accuracy for eight methods. Methods positioned towards the bottom left corner are indicative of greater computational efficiency. The impact-increment and SS methods can improve the accuracy and computational speed, respectively. Therefore, combining the SS and impact-increment methods allows SSIISE to outperform the conventional SE method in both computational time and accuracy. The MCS method, a conventional technique for power system reliability assessment, is also included for comparison. As shown in Fig.

5, the computational speed of SSMCS is approximately 100 times faster than that of the MCS method. Moreover, the CEMCS method is a popular advanced method that can reduce samples and increase the convergence speed of MCS. By integrating the SS method with CEMCS, further improvements in computational efficiency are achieved. As demonstrated in Table II, the SSCEMCS method takes only about 10s to evaluate the reliability of the RTS-79 system.

Table. II Reliability assessment results of eight methods (RTS-79)

ζ_{re} (%)	Method	EENS(MWh/y)		OPF Number*	CPU Time(s)
		Value	Relative Error (%)		
0	**Baseline**	531.36	-	-	-
	MCS	527.56	0.72	31290000	34814
	SSMCS	527.56	0.72	9646	329
	CEMCS	527.42	0.74	298000	326
	SSCEMCS	527.42	0.74	874	13
	SE	308.41	41.96	24478200	24354
	SSSE	308.41	41.96	161	119
	IISE	484.81	8.76	24478200	24373
	SSIISE	484.81	8.76	161	142
5	**Baseline**	1061.14	-	-	-
	MCS	1060.62	0.05	16110000	17868
	SSMCS	1060.62	0.05	3313	122
	CEMCS	1076.60	1.46	185300	206
	SSCEMCS	1076.60	1.46	951	10
	SE	673.10	36.57	24478200	24419
	SSSE	673.10	36.57	196	126
	IISE	976.15	8.01	24478200	24435
	SSIISE	976.15	8.01	196	147
10	**Baseline**	2217.43	-	-	-
	MCS	2185.37	1.45	7970000	8815
	SSMCS	2185.37	1.45	1318	114
	CEMCS	2236.44	0.86	160200	179
	SSCEMCS	2236.44	0.86	1000	10
	SE	1505.18	32.12	24478200	24414
	SSSE	1505.18	32.12	350	146
	IISE	2011.97	9.27	24478200	24440
	SSIISE	2011.97	9.27	350	169
15	**Baseline**	4757.97	-	-	-
	MCS	4718.36	0.83	3760000	4158
	SSMCS	4718.36	0.83	1947	46
	CEMCS	4783.93	0.55	116500	126
	SSCEMCS	4783.93	0.55	1291	10
	SE	3410.00	28.33	24478200	24431
	SSSE	3410.00	28.33	505	170
	IISE	4241.58	10.85	24478200	24434
	SSIISE	4241.58	10.85	505	194

***OPF number** is the number of using optimization algorithms to solve the DC OPF problem, and it is also the number of state similarity categories.

As shown in Table II, the computational efficiency of the SS method slightly decreases with higher renewable penetration. Specifically, at 0% renewable penetration, the numbers of OPF calculations per 10,000 scenarios are 3.08 for SSMCS and 29.32 for SSCEMCS, whereas at 15% penetration, they increase to 5.18 and 110.82,

respectively. A similar increasing trend is observed for both the SE and IISE methods. This behavior occurs because the inherent variability of renewable generation alters the set of active constraints, making it more difficult to match new states to existing state-similarity categories. Nevertheless, despite the increase in OPF calculations at higher renewable levels, the proposed SS method continues to provide substantial improvements in computational efficiency.

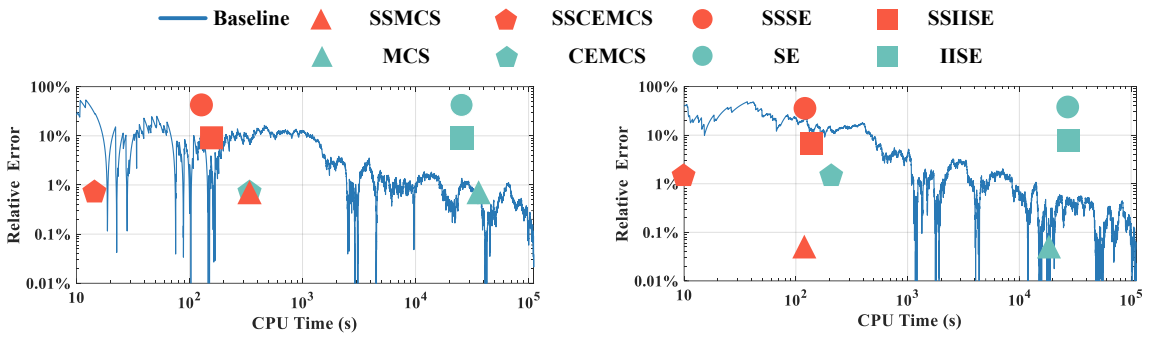

(a) ζ_{re} = 0 % (b) ζ_{re} = 5 %

Fig. 5. Computational efficiencies of eight methods (RTS-79).

4.1.2 Comparison Results Analysis

Compared with other advanced methods, the proposed SS method can incorporate all types of system states into the accelerating calculation process. Based on the previous study [37], the calculation speed is increased by 39.12 times by accelerating the evaluations of load and renewable generation states. Furthermore, large numbers of OPF computations of transmission line (TL) and generation (G) states are replaced with the active-constraints-based equations for the proposed SSIISE and SSCEMCS methods. In this way, SSIISE can reduce the OPF number from 299919 to 22157, thereby improving the efficiency by 3.33 times. As shown in Table III, the improvement with SSCEMCS is less than that of SSIISE. This is because the cross-entropy method filters out a large number of states that have minimal impact on system reliability, and the sampled states of SSCEMCS exhibit more state similarities. However, over 97% of OPF computations are still avoided, leading to a significant efficiency improvement in the CEMCS due to the SS method.

Table III demonstrates the benefits of dynamic sorting and fast matrix inversion techniques. In this case, t_1 = 2, t_2 = 50, and N_{tri} = 1. Take SSIISE as an example, the dynamic sorting technique reduces the computing time from 187s to 142s. However, the fast matrix inversion technique has little impact on the SSIISE method. It only takes

0.45s to invert the matrix for the SSIISE, thus the saved time can be ignored. On the other hand, SSCEMCS requires more time to invert the matrix due to the frequently changing topology in the sample states. Therefore, the speedup of SSCEMCS is increased from 19.18 to 25.08 by using the fast matrix inversion technique.

Table. III Performance comparisons of the proposed methods (RTS-79)

State	Method	EENS (MWh/y)	OPF Number	CPU Time(s)	Speedup
-	IISE	484.81	24478200	24373	1.0
LR	SSIISE [37]	484.81	299919	623	39.12
LR, G	SSIISE	484.81	24706	192	126.84
LR, G, TL	SSIISE	484.81	22157	187	130.24
LR, G, TL	SSIISE & Sort	484.81	161	142	171.51
LR, G, TL	SSIISE & Sort & Inv	484.81	161	142	171.51
-	CEMCS	527.42	298000	326	1.0
LR	SSCEMCS	527.42	57867	84	3.88
LR, G	SSCEMCS	527.42	29769	47	6.94
LR, G, TL	SSCEMCS	527.42	8868	39	8.36
LR, G, TL	SSCEMCS & Sort	527.42	874	17	19.18
LR, G, TL	SSCEMCS & Sort & Inv	527.42	874	13	25.08

***LR**: Load and Renewable Generation states. **Sort**: Dynamic sorting technique. **Inv**: Fast matrix inversion technique.

Fig. 6 shows the computational time of each process in three methods. M1, M2, and M3 represent the methods of SSCEMCS, SSCEMCS & Sort, and SSCEMCS & Sort & Inv, respectively. The matching process is used to match the system state with a similarity category in the state similarity set. Matched states are calculated using active-constraints-based equations, while unmatched states are evaluated using optimization algorithms. Compared to M1, the number of matching processes in M2 decreases from 1.63×10^6 to 4.26×10^5, and the OPF number decreases from 8868 to 874. Therefore, the dynamic sorting technique can significantly reduce the time of matching, inversing, and OPF processes. For M2 and M3, the fast matrix inversion technique can nearly double the calculation speed of the matrix inversion process. The other processes, which include OPF modeling and state selection, take a similar amount of time across M1, M2, and M3, as the number of system states is consistent.

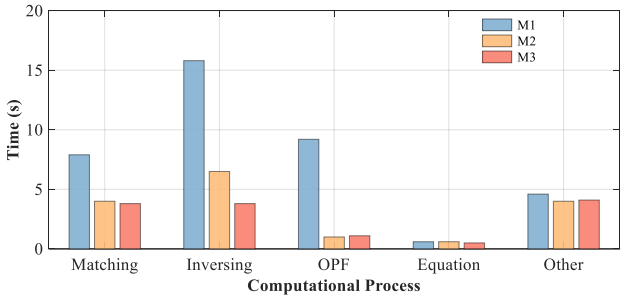

Fig. 6. Computational time of three methods (RTS-79).

4.1.3 Results of One Load Curve Case

To verify the accuracy of the proposed method, it is applied to the one load curve case [44], the results of which

have been reported in various studies. As shown in Table IV, the reliability results of the proposed SS method are nearly identical to those provided in [32], with a negligible discrepancy of only 0.48%. This minor variance can be attributed to the inherent randomness associated with MCS sampling. Therefore, the reliability results of the proposed method are considered acceptable.

Table. IV Reliability assessment results of one load curve case (RTS-79)

Method	EENS(MWh/y)	OPF Number	CPU Time(s)
CEMCS [32]	1293	-	-
MCS	1299.23	15560000	16528
SSMCS	1299.23	6370	275
CEMCS	1282.65	325000	353
SSCEMCS	1282.65	1248	19
SE	1056.56	24478200	24161
SSSE	1056.56	886	136
IISE	1298.92	24478200	24184
SSIISE	1298.92	886	158

4.2. Case II: Results on the RTS-96 System

RTS-96 system [45] consists of 73 buses, 99 generation units, and 120 branches. The total generation capacity is 10 215 MW and the peak load is 8550 MW. This system utilizes the same load and renewable energy curves as the RTS-79 system, but to enhance the MCS sampling efficiency, the load curves values are increased by 15%. When $\zeta_{re} = 0$, the results of 2×10^8 sampled states are used as the baseline, with $N_T = 7$. If $\zeta_{re} > 0$, the results of 1×10^8 sampled states serve as the benchmark, with $N_T = 6$. The other parameters remain the same as in Case I. The reliability assessment results for the RTS-96 system are presented in Table V to demonstrate the scalability of the proposed SS method.

4.2.1 Accuracy and Efficiency

In the RTS-96 system, the SS method can still significantly improve the computational efficiency of MCS, CEMCS, SE, and IISE methods. Less than 1% of the states require calculation through optimization algorithms, resulting in a speedup of more than 10 times without sacrificing accuracy. As shown in the $\zeta_{re} = 0$ of Table V, the computational time can be reduced from 3.85×10^5s to 5617s by SSMCS, and further reduced to 371s by SSCEMCS.

4.2.2 Comparison Results Analysis

The performance comparisons of the proposed SSCEMCS method for the RTS-96 system are presented in Table VI. By utilizing all types of states to match a state similarity category, the SS method achieves a speedup of 6.05 times, reducing the OPF count from 2,765,000 to 90,672. When the accelerated states are the load and renewable

generation (LR) states, the speedup of SSCEMCS in Table III is 3.88, while it is only 1.13 in the RTS-96 system. This is because the sampled states in the RTS-96 system are usually different in component states, and only a few sampled states can be analyzed quickly based on LR variations.

Table. V Reliability assessment results of eight methods (RTS-96)

ζ_{re} (%)	Method	EENS(MWh/y)		OPF Number	CPU Time(s)
		Value	Relative Error (%)		
0	**Baseline**	201.94	-	-	-
	MCS	200.21	0.86	143430000	385225
	SSMCS	200.21	0.86	22999	5617
	CEMCS	201.44	0.25	2765000	7903
	SSCEMCS	201.44	0.25	7673	371
	SE	6.98	96.54	742650100	1880728
	SSSE	6.98	96.54	1191	15146
	IISE	132.89	34.19	742650100	1881465
	SSIISE	132.89	34.19	1191	15879
5	**Baseline**	1035.34	-	-	-
	MCS	1031.70	0.35	30400000	80269
	SSMCS	1031.70	0.35	5642	1534
	CEMCS	1033.82	0.15	1230000	3446
	SSCEMCS	1033.82	0.15	11101	263
	SE	37.88	96.34	663982400	1676673
	SSSE	37.88	96.34	577	16331
	IISE	652.45	36.98	663982400	1676974
	SSIISE	652.45	36.98	577	16537
10	**Baseline**	5187.40	-	-	-
	MCS	5262.79	1.45	6620000	17557
	SSMCS	5262.79	1.45	4681	436
	CEMCS	5204.23	0.32	915000	2559
	SSCEMCS	5204.23	0.32	8586	173
	SE	501.63	90.33	663982400	1701297
	SSSE	501.63	90.33	988	17589
	IISE	3505.95	32.41	663982400	1701599
	SSIISE	3505.95	32.41	988	17889
15	**Baseline**	24043.43	-	-	-
	MCS	24520.65	1.98	1600000	4395
	SSMCS	24520.65	1.98	2549	168
	CEMCS	23975.39	0.28	579000	1579
	SSCEMCS	23975.39	0.28	3888	102
	SE	4245.93	82.34	663982400	1702145
	SSSE	4245.93	82.34	1751	18121
	IISE	16669.44	30.67	663982400	1702440
	SSIISE	16669.44	30.67	1751	18408

When considering the TL states, the OPF number is reduced from 92129 to 90672, but the computing time increases from 1147s to 1306s. This is due to the high computational cost associated with matrix inversion during the matching process. This highlights the importance of dynamic sorting and fast matrix inversion techniques in the proposed SS methods, especially for large-scale systems. Table VI illustrates the impact of these enhanced techniques on the SSCEMCS method for the RTS-96 system. The dynamic sorting technique reduces the computing time to 494s, while the fast matrix inversion technique further decreases it to 371s.

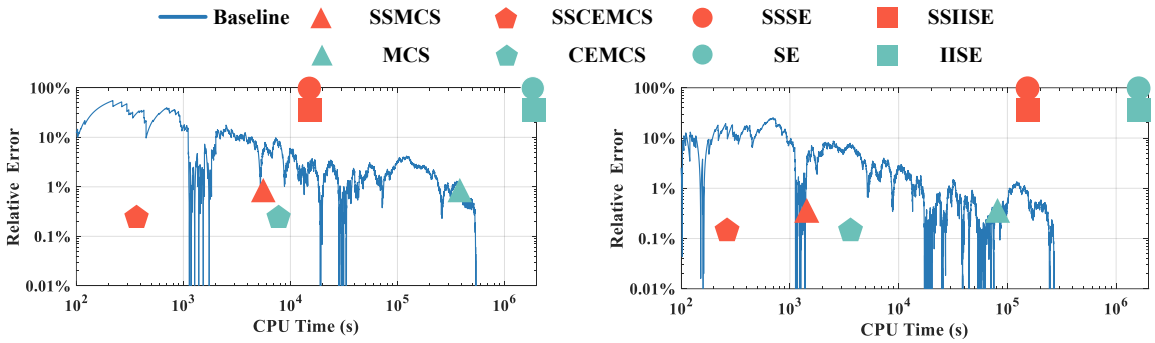

(a) ζ_{re} = 0 % (b) ζ_{re} = 5 %

Fig. 7. Computational efficiencies of eight methods (RTS-96).

Table. VI Performance comparisons of the proposed methods (RTS-96)

State	Method	EENS (MWh/y)	OPF Number	CPU Time(s)	Speedup
-	CEMCS	201.44	2765000	7903	1.0
LR	SSCEMCS	201.44	2551620	6979	1.13
LR + G	SSCEMCS	201.44	92129	1147	6.89
LR + G + TL	SSCEMCS	201.44	90672	1306	6.05
LR + G + TL	SSCEMCS & Sort	201.44	7673	494	15.99
LR + G + TL	SSCEMCS & Sort & Inv	201.44	7673	371	21.28

4.3. Case III: Results on the Brazilian System

Brazilian system [46], an equivalent network of the southern region of Brazil, consists of 242 buses, 53 generation units, and 489 branches. The total generation capacity is 208 388 MW and the peak load is 185 276 MW. The results of 5×10^7 sampled states are used as the baseline, ζ_{re} = 15%, and N_T = 4. The other parameters are consistent with Case I.

Table. VII Reliability assessment results of eight methods (BRAZILIAN)

Method	EENS(MWh/y)		OPF Number	CPU Time(s)
	Value	Relative Error (%)		
Baseline	2165.56	-	-	-
MCS	2193.60	1.29	30880000	385099
SSMCS	2193.60	1.29	11522	15035
CEMCS	2178.92	0.62	2263000	29962
SSCEMCS	2178.92	0.62	22404	2229
SE	614.21	71.64	46340500	527245
SSSE	614.21	71.64	27448	10554
IISE	1760.31	18.71	46340500	527249
SSIISE	1760.31	18.71	27448	10558

As shown in Table VII, compared with traditional MCS and SE methods, the proposed SS method remarkably improves the computational efficiency by over 26 times. Also, the proposed SSCEMCS method can further decrease the computation time to 2229s.

Moreover, the impact of system size on the number of state similarity categories is analyzed. The number

of state similarity categories serves as an indicator of the acceleration performance of the proposed method. A smaller number of categories implies a higher degree of similarity among multiple system states, enabling their optimal solutions to be rapidly obtained through solving equations. Conversely, a larger number of state similarity categories indicates lower similarity, thereby limiting the acceleration potential of the SS method. The OPF number can be adopted as a proxy for the number of state similarity categories. In general, this number increases with system size. As shown in Tables II, V, and VII, for instance, under the SSMCS method, the numbers of state similarity categories for the RTS-79, RTS-96, and Brazilian systems are 1,318, 4,681, and 11,522, respectively.

5. Conclusion

This paper proposes a state-similarity-based method for efficient reliability assessment in power systems. The active constraints can be used as the state similarity features to calculate optimal load curtailment by solving linear equations, rather than the time-consuming OPF optimizations. The method accounts for all types of system states, including transmission line outages and renewable energy variations, in its accelerated calculation processes. The results demonstrate that the proposed SS method is 20 to 200 times faster than traditional MCS and SE methods, eliminating the need for OPF optimizations in more than 99% of system states. Additionally, the dynamic sorting and fast matrix inversion techniques improve the matching efficiency by 2~3 times. The SS method can also be integrated with other advanced methods, such as the CE method, to further improve overall efficiency, as it focuses primarily on system state analysis. However, the current SS method is limited to linear optimization formulations and cannot yet be directly applied to nonlinear problems. In future work, we plan to extend the SS framework to handle more complex OPF models that incorporate time-coupling constraints of flexible resources, thereby enabling a more comprehensive analysis of the evolving challenges in modern power systems.

The source code and data are available at: https:// github.com/tjuZeyuLiu/OA-Reliability-Assessment.

Reference

[1] Arabzadeh V, Frank R. Creating a renewable energy-powered energy system: Extreme scenarios and novel solutions for large-scale renewable power integration. Applied Energy, 2024, 374: 124088.

[2] Fang Y, Han J, Du E, et al. Electric energy system planning considering chronological renewable generation variability and uncertainty. Applied Energy, 2024, 373: 123961.

[3] Qu J, Hou K, Liu Z, et al. A hybrid time-and-event-driven strategy for integrated community energy system planning. Applied Energy, 2025, 384: 125274.

[4] Yang H, Jiang P, Wang Y, et al. A fuzzy intelligent forecasting system based on combined fuzzification strategy and improved optimization algorithm for renewable energy power generation. Applied Energy, 2022, 325: 119849.

[5] Zhang D, Shafiullah G M, Das C K, et al. Optimal allocation of battery energy storage systems to improve system reliability and voltage and frequency stability in weak grids. Applied energy, 2025, 377: 124541.

[6] Alanazi M, Alanazi A, Akbari M A, et al. A non-simulation-based linear model for analytical reliability evaluation of radial distribution systems considering renewable DGs. Applied Energy, 2023, 342: 121153.

[7] Chen H, Pilong C, Rocha-Garrido P, et al. Grid resilience with high renewable penetration: A PJM approach. IEEE Transactions on Sustainable Energy, 2022, 14(2): 1169-1177.

[8] Li W. Reliability assessment of electric power systems using Monte Carlo methods. Springer Science & Business Media, 2013.

[9] Gbadamosi S L, Nwulu N I. Reliability assessment of composite generation and transmission expansion planning incorporating renewable energy sources. Journal of Renewable and Sustainable Energy, 2020, 12(2).

[10] Ding Y, Singh C, Goel L, et al. Short-term and medium-term reliability evaluation for power systems with high penetration of wind power. IEEE Transactions on Sustainable Energy, 2014, 5(3): 896-906.

[11] Qu J, Liu Z, Hou K, et al. Joint planning of economy and reliability for integrated community energy systems: A similarity-based massive scenario optimization approach. Applied Energy, 2025, 381: 125054.

[12] Liu H, Sun Y, Wang P, et al. A novel state selection technique for power system reliability evaluation. Electric power systems research, 2008, 78(6): 1019-1027.

[13] Jia Y, Wang P, Han X, et al. A fast contingency screening technique for generation system reliability evaluation. IEEE Transactions on Power Systems, 2013, 28(4): 4127-4133.

[14] Hou K, Jia H, Li X, et al. Impact-increment based decoupled reliability assessment approach for composite generation and transmission systems. IET Generation, Transmission & Distribution, 2018, 12(3): 586-595.

[15] Tomasson E, Söder L. Generation adequacy analysis of multi-area power systems with a high share of wind power. IEEE Transactions on Power Systems, 2017, 33(4): 3854-3862.

[16] Fang K, Li C, Tang Y, et al. China's pathways to peak carbon emissions: New insights from various industrial sectors. Applied Energy, 2022, 306: 118039.

[17] Mardones C, Alvial E. Evaluation of a carbon tax in Costa Rica linking a demand system focused on energy goods and an input-output model. Applied Energy, 2024, 363: 123078.

[18] Tomasson E, Söder L. Improved importance sampling for reliability evaluation of composite power systems. IEEE Transactions on Power Systems, 2016, 32(3): 2426-2434.

[19] He X, Ding T, Zhang X, et al. A robust reliability evaluation model with sequential acceleration method for power systems considering renewable energy temporal-spatial correlation. Applied Energy, 2023, 340: 120996.

[20] Hu Z, Xu Y, Korkali M, et al. A Bayesian approach for estimating uncertainty in stochastic economic dispatch considering wind power penetration. IEEE Transactions on Sustainable Energy, 2020, 12(1): 671-681.

[21] Hou K, Jia H, Xu X, et al. A continuous time Markov chain based sequential analytical approach for composite power system reliability assessment. IEEE Transactions on Power Systems, 2015, 31(1): 738-748.

[22] Hua B, Bie Z, Au S K, et al. Extracting rare failure events in composite system reliability evaluation via subset simulation. IEEE Transactions on Power Systems, 2014, 30(2): 753-762.
[23] Zhao Y, Tang Y, Li W, et al. Composite power system reliability evaluation based on enhanced sequential cross-entropy Monte Carlo simulation. IEEE Transactions on Power Systems, 2019, 34(5): 3891-3901.
[24] Jia Y, Bai X, Zheng L, et al. ConvOPF-DOP: A data-driven method for solving AC-OPF based on CNN considering different operation patterns. IEEE Transactions on Power Systems, 2022, 38(1): 853-860.
[25] Zhou M, Chen M, Low S H. DeepOPF-FT: One deep neural network for multiple AC-OPF problems with flexible topology. IEEE Transactions on Power Systems, 2022, 38(1): 964-967.
[26] Van Nooten C C, Van de Poll T, Füllhase S, et al. Graph neural networks for assessing the reliability of the medium-voltage grid. Applied Energy, 2025, 384: 125401.
[27] Liu X, Gao M, Yu J, et al. Multi-Kernel Collaborative Graph Convolution Neural Network for Operational Reliability Assessment Considering Varying Topologies[J]. Journal of Modern Power Systems and Clean Energy, 2025.
[28] Chatzivasileiadis S, Venzke A, Stiasny J, et al. Machine learning in power systems: Is it time to trust it?. IEEE Power and Energy Magazine, 2022, 20(3): 32-41.
[29] Liu Z, Zhu L, Hou K, et al. A State-similarity-based fast reliability assessment for power systems with variations of generation and load. IEEE Transactions on Power Systems, 2024. doi: 10.1109/TPWRS.2024.3415367.
[30] Liao B. Application of linear programming sensitivity analysis in reliability evaluation of bulk power system. International Journal of Hydroelectric Energy, 1991, 9(2): 154-160.
[31] Safdarian A, FOTUHI-FIRUZABAD M, Aminifar F. Composite power system adequacy assessment based on postoptimal analysis. Turkish Journal of Electrical Engineering and Computer Sciences, 2013, 21(1): 90-106.
[32] Yong P, Zhang N, Kang C, et al. MPLP-based fast power system reliability evaluation using transmission line status dictionary. IEEE Transactions on Power Systems, 2018, 34(2): 1630-1640.
[33] Qu J, Xu K, Hou K, et al. Reliable and Economic Operation of Regional-Community Integrated Energy Systems: A Hybrid Game Approach Based on State Similarity. Energy, 2025: 137983.
[34] Liu Z, Tang P, Hou K, et al. A Lagrange-multiplier-based reliability assessment for power systems considering topology and injection uncertainties. IEEE transactions on power systems, 2023, 39(1): 1178-1189.
[35] Luo F, Ge N, Xu J. Analytical Calculation Method for Power Supply Reliability of Distribution Systems With Multiple Tie Lines. IEEE Transactions on Reliability, 2025.
[36] Liu Z, Zhu L, Hou K, et al. A State-similarity-based fast reliability assessment for power systems with variations of generation and load. IEEE Transactions on Power Systems, 2024.
[37] Liu Z, Hou K, Jia H, et al. A Lagrange multiplier based state enumeration reliability assessment for power systems with multiple types of loads and renewable generations. IEEE Transactions on Power Systems, 2020, 36(4): 3260-3270.
[38] Abedi A, Gaudard L, Romerio F. Power flow-based approaches to assess vulnerability, reliability, and contingency of the power systems: The benefits and limitations. Reliability Engineering & System Safety, 2020, 201: 106961.
[39] Liu Y, Wang Y, Yong P, et al. Fast power system cascading failure path searching with high wind power penetration. IEEE Transactions on Sustainable Energy, 2019, 11(4): 2274-2283.
[40] Wu T, Wang J. Reliability evaluation for integrated electricity-gas systems considering hydrogen. IEEE Transactions on Sustainable Energy, 2022, 14(2): 920-934.
[41] Cao M, Shao C, Hu B, et al. Reliability assessment of integrated energy systems considering emergency dispatch based on dynamic optimal energy flow. IEEE transactions on sustainable energy, 2021, 13(1): 290-301.
[42] D. G. Luenberger, Linear and nonlinear programming. New York, NY, USA: Springer, 2005.
[43] Gene H. Golub, Charles F. Van Loan, Matrix computations. NJ, Englewood Cliffs: Johns Hopkins University Press, 1983.
[44] Subcommittee P M. IEEE reliability test system. IEEE Transactions on power apparatus and systems, 1979 (6): 2047-2054.

[45] Grigg C, Wong P, Albrecht P, et al. The IEEE reliability test system-1996. A report prepared by the reliability test system task force of the application of probability methods subcommittee. IEEE Transactions on power systems, 1999, 14(3): 1010-1020.
[46] Brazilian system reliability data, Github, Aug. 2021. [Online]. Available: https://github.com/ProfFernando Assis/ReliabilityData.
[47] Hourly load data by area and region from January 1, 2011 to December 31, 2016, AESO, Apr. 2018. [Online]. Available: https://www.aeso.ca/.
[48] Solar power data for integration studies, NREL, 2007. [Online]. Available: https://www.nrel.gov/grid/solar-power-data.html.
[49] Eastern and western wind integration data sets, NREL, 2014. [Online]. Available: https://www.nrel.gov/grid/ eastern-western-wind-data.html.